Journal of Data Acquisition and Processing
ISSN: 1004-9037
https://sjcjycl.cn/
DOI: 10.5281/zenodo.777624

A CRITICAL STUDY ON SUB-MICROSPHERS POSITIVE ELECTRODES FOR SOLID STATE ASYMMETRIC SUPERCAPACITORS

Mr.Serfraz Najeer Shaikh
Research Scholar, Electronics and Communication Engg.Dr.APJ Abdul KalamUniversity, Indore, India, serfrazshaikh@gmail.com

Dr.Rahul Mishra
Electronics and Communication Engg. Dr.APJ Abdul KalamUniversity, Indore, India
rahulmishra@aku.ac.in

ABSTRACT

The solid-state "Mn0.75Ni0.25CO3/GNS asymmetric supercapacitor had a specific capacitance of 46-22 F g-1 at varied current densities (0.5-9.0 A g-1). The Mn0.75Ni0.25CO3/GNS asymmetric supercapacitor device as-fabricated demonstrated a power density of 499 W kg-1 at a high specific energy density of 25 Wh kg-1, and the solid-state ASC maintained 88% capacitance even after 7500 cycles, which is another benefit and suitable for commercial applications. Electrochemical impedance spectroscopy experiments were performed on all the materials produced in the half-cell, three-electrode, and two-electrode systems. The LMNCO-950 electrode represented the lowest Rs (2.18) and Rct (39.18) values, confirming the material is relatively stable and excellent. The Li+ diffusion co-efficient of LMNCO-950 (2.783 x10-15) is significantly higher than the LMNCO-800 (1.367 x10-15), LMNCO-900 (2.767 x10-15), and LMNCO-1000 (1.647 x10-15) samples. The obtained Rct values for H-CMO at the third and 500th cycles are 285 and 396, 267 and 355 for P-CMO, and 186 and 262 for GW-P-CMO. The GW-P-CMO electrode outperformed the other two in terms of capacity retention and had a lower Rct. The best Li-ion diffusion coefficient, lowest Rs and Rct values, and very stable material interfaces even after extended cycling without disintegration are all indicators of this. The porous, smaller particle size, and high active surface area natured Mn based nano structures, which support the greater electrode/electrolyte interface and, consequently, good electrochemical performance, are responsible for the lowered Rct values. Another option is the quicker transfer of charged particles between the electrode and electrolyte. These material properties improve electrochemical performances by resulting in high specific capacitance and superior capacity retention properties. Cyclic stability is crucial for energy storage applications and is required for renewable energy storage systems and hybrid electric vehicles."

KEY WORDS: Sub-Microsphers, Positive, Electrodes, Solid State, Asymmetric Supercapacitors, Low-Cost Metal Oxide.

1. INTRODUCTION

Super capacitors and batteries, specifically, are progressing quickly regarding advancement of minimal expense, high-energy thickness, "and power thickness electrochemical energy stockpiling frameworks viable with atomic, sun oriented, and wind energy assets [1-3]. The previous one meets all necessities. As opposed to customary capacitors, which have high power however lower energy thickness, super capacitors have high power and energy thickness alongside long haul cyclic steadiness, working security, and harmless to the ecosystem and reasonable super capacitors [4-7]. Electrical twofold layer capacitors (EDLCs) and pseudo capacitors are two unique types of super capacitors that can be recognized by how they store charge [8, 9]. While there is no redox response in the terminal materials of EDLC, the specific capacitance in pseudocapacitors is very low and is subject to the cathode dynamic surface region, where the outer layer of the cathode materials will experience a reversible redox (Faradaic) response during the charge-release processes, particularly in the metal oxide or leading polymer of choice. Finding pseudo capacitor materials (change metal oxides) that can store more charges for a longer period of time without experiencing critical energy misfortune is crucial because EDLC has a reduced capacitance [10, 11].Because of their various oxidation states and straightforwardness of production, progress metal oxides have drawn critical interest as pseudocapacitor materials. RuO2.XH2O is a notable pseudocapacitor produced using various metal oxides that performs well, has a high unambiguous capacitance (760 F g-1), and has a long cycle life. Glassine applications were anyway restricted by its low porosity, harmfulness, shortage of its crude fixings, and fast decrease in power thickness at high charge-release current cutoff points [12,13]. The objective of numerous electrochemical examinations is to find a minimal expense metal oxide to supplant RuO2. As of late, a lot of consideration has been paid to change metal mixtures with different morphologies that include nickel, cobalt, and manganese. Interphase multiphase Fe-doped MnO2 nanostructures were made and analyzed electrochemically by Wang and his colleagues [14]. NiCo2O4@NiWO3 nanowire exhibits were made by Chen et al. also, can be utilized as an electroactive material for super capacitors since they give great limit maintenance and long haul cycle security [15]. On nickel froth, Zhang et al. made 3D Co3O4-Ni3(VO4)2 heterostructured nanorods with better electrochemical attributes for supercapacitor anodes that perform very well generally electrochemically [16]." These high unambiguous surface region temporary terminal materials have been utilized widely in pseudocapacitor applications [17-19]. A couple of terminals with metal carbonates are accounted for in the previously mentioned papers, which for the most part showed the utilization of change metal oxides, sulfides, and hydroxides as the supercapacitors cathode materials [20-26]. "As far as we could possibly know, in any case, this is whenever that we first have reported the blend of Mn0.75Ni0.25CO3 nano/sub-microspheres for use as terminal materials in strong state uneven supercapacitor (ASC) applications. Since it is harmless to the ecosystem, this material can be applied to an assortment of capacitance applications. Gigantic endeavors have been made to make energy capacity gadgets that are naturally harmless, very steady, and low weight for use with batteries and supercapacitors in the advanced electronic enterprises [1-3]. Supercapacitors are preferred electrochemical energy stockpiling gadgets over regular energy stockpiling gadgets since they have more noteworthy cycle solidness, high power thickness, and rate capacity. Contingent upon how they store their

charge, supercapacitors can be partitioned into three classes: electrical twofold layer capacitors (EDLC), pseudo-capacitors, and half and half capacitors. While energy in pseudocapacitors and mixture capacitors is shown by a Faradic response similar to a battery-powered battery, energy in EDLCs is made on the cathode/electrolyte interface by electrostatic fascination with the gathering of charges. At the point when EDLC anode materials such graphite, carbon, initiated carbon, and directing polymer materials are delivered with metal oxides, they show further developed pseudocapacitance characteristics. The pseudocapacitance materials have great capacitance maintenance, fast and reversible redox responses, and high energy densities, which are all pivotal for energy capacity applications [4,5]. These materials' physiochemical highlights, areas of strength for like conductivity, huge surface region, low thickness, and shell penetrability, will in this way be worked on by forming them into permeable nano-architectured terminal materials. Moreover, for the different expected utilizes, the amalgamation of permeable/empty circles [6-8], solid shapes [9-10], polyhedrons [11], bowls [12], and their control into twofold layer shells [12,13], as well as multi-facet shells [14,15], was attempted."

Mesoporous nano/miniature estimated particles have been concentrated on to increment capacitance, decline the movement length for the electrons second, and work on the dynamic materials by use. The production of permeable Mn2O3 structures utilizing different engineered strategies has been recorded in various scholastic examinations."The aqueous procedure was utilized to make permeable Mn2O3 nanocubes, which showed explicit capacitance of 191 F g-1 and capacitance maintenance of 58.6% in Na2SO4 electrolyte [17]. Because of their high surface region, capacity to relieve a portion of the volume change during the charge-release interaction, and capacity to build the contact region of the electro-dynamic surface with electrolyte, these permeable alterations have been viewed as a promising construction for the elite presentation cathode materials for supercapacitors. Subsequently, during charge-release cycling, the materials can support an expanded explicit current. Also, during charge/release processes, the anode material can endure volume development and compression.

The significance of planning and making permeable Mn2O3 nanospheres and nanocubes with nano-design for supercapacitor applications is in this way featured in the ongoing section. The aqueous methodology was utilized to make the layout free circles and shapes of Mn2O3 that self-gathered with help from CO32-and SO42-particles. To build the dynamic locales for the expanded Faradic response, the porosity of the Mn2O3 circles and 3D squares was created utilizing calcinations. With a three cathode framework and a LiNO3 electrolyte, the electrochemical exhibition of the created permeable Mn2O3 nanospheres and nanocubes terminal was inspected. Brilliant explicit capacitance upsides of 345 F g-1 and 321 F g-1 at 0.2 A g-1 were found. To fabricate the PVA-LiNO3 strong state electrolyte, two terminal frameworks were utilized interestingly. The combined Mn2O3 (positive) and rGO (negative) cathodes exhibited and incredibly improved explicit capacitance. This gathering can perform at incredibly high power and energy densities.

In this review, we utilized a straightforward sodium bicarbonate-helped co-precipitation way to deal with Make Mn1-xNixCO3 (x-0, 0.20, 0.25, and 0.30) nano/sub-microspheres with regulated shape. The transparent structure, usable clusters, and shape of the as-arranged

materials were assessed using X-beam diffraction (XRD), Fourier transform infrared spectroscopy (FT-IR), scanning electron microscopy (SEM), and transmission electron microscopy (TEM). According to the electrochemical investigations, the Mn0.75Ni0.25CO3 nano/sub-microspheres exhibit increased explicit capacitance of 364 F g-1 at a continuous thickness of 1A g-1, high rate capacity, and unmatched cycle soundness. Furthermore, for the strong state ASC with Mn0.75Ni0.25CO3/GNS arrangement, Mn0.75Ni0.25CO3 nano/sub-microspheres" and graphene nanosheets (GNS) were used as the positive and negative terminals. The strong state ASC Mn0.75Ni0.25CO3/GNS device is particularly effective, with a power thickness of 499 W kg-1 and a high energy thickness of 25 Wh kg-1. A structure with the custom Mn0.75Ni0.25CO3/GNS configuration may be used in industry.

2. RESEARCH METHODOLOGY

"Synthesis of $Mn_{1-x}Ni_xCO_3$ (x=0.0, 0.20, 0.25 and 0.30) nano/sub-microspheres"

"It was easy to make Mn1-xNixCO3 nano/sub-microspheres utilizing the co-precipitation approach. Commonly, sodium bicarbonate (10 mM) was broken up independently in twofold distiller water while manganese sulfate (0.75 mmol) and nickel sulfate (0.25 mM) were disintegrated in a similar measure of water (70 ml). The MnSO4 and NiSO4 arrangements were then steadily given ethanol (7 ml) while being continually mixed. The previously mentioned combination was then added to the NaHCO3 arrangement at room temperature after it had completely disintegrated. The response arrangement became green following 5 minutes. This showed that Mn0.75Ni0.25CO3 nano/sub-microspheres were at first shaped after the combination was persistently unsettled for three hours at room temperature. To eliminate impurities, the delivered Mn0.75Ni0.25CO3 nano/sub-microspheres were isolated by filtration and over and again washed with ultrapure water and ethanol. To dispose of the water particles that had been adsorbed on the outer layer of the Mn0.75Ni0.25CO3 nano/sub-microspheres, they were dried at 120 °C for 12 hours. A similar cycle was utilized to make Mn1-xNixCO3 nano/sub-microspheres (x=0.0, 0.20, 0.25, and 0.30) by adding the perfect proportion of Mn and Ni particle sources."

2.1 ELECTROCHEMICAL MEASUREMENTS

The electrochemical characteristics of the orchestrated Mn1-xNixCO3 (x=0.0, 0.20, 0.25, and 0.30) nano/sub-microsphere anodes were examined using three terminal frameworks in cyclic voltammetry (CV), galvanostatic charge-release (GCD), and electrochemical impedance spectroscopy tests. In order to create the working cathode, the provided Mn1-xNixCO3 nano/sub-microsphere materials (dynamic materials-70%) were combined with acetylene dark (20%), polyvinylidene fluoride (PVDF) (10%), fastener, and a few drops of n-methyl-2-pyrrolidone (NMP) as the dissolvable. "A nickel froth substrate (1 cm X 1 cm) was covered with the dynamic substance (1.5 mg), which was then dried at 90 °C for 10 hours. This went about as the functioning terminal, and the reference and counter cathodes were made of immersed calomel (SCE) and platinum wire, separately. In 1 M of Na2SO4 watery

arrangements electrolyte, the anode for electrochemical portrayals was evaluated at different output rates and ebb and flow densities.

A cellulosic paper separator and two cuts of dynamic materials covered nickel froth (2 X 1 cm) are remembered for the created strong state ASC gadget. The two-terminal framework (1.2 mg) employed the Mn0.75Ni0.25CO3 nano/sub-microspheres as the positive cathode, and the graphene nanosheet (GNS), which was produced by adhering 20% acetylene dark and 10% PVDF in NMP slurry on a nickel froth, as the negative terminal (3.8 mg). After fervently whirling 2 g of PVA powder into 20 ml of deionized water at 95°C to create the strong state electrolyte, an unmistakable arrangement was created. In order to create the PVA-Na2SO4 strong state gel, 1 g of Na2SO4 was subsequently added to the basic arrangement discussed before while being blended for 30 minutes. The positive anode (Mn0.75Ni0.25CO3 nano/sub-microspheres) and negative terminal (GNS) separator were immersed in the PVA-Na2SO4 strong state solution for 5 minutes before being removed, constructed, and placed under vacuum to create the strong state ASC. The greatest capacitance and working expected window, which were resolved utilizing the accompanying charge balance condition [27], were utilized to decide the best mass proportion (m+/m) between the positive and negative cathodes."

$$q^{+} = q^{-}$$

$$q = m \times c \times v$$

$$m^{+}/m^{-} = c^{-}v^{-} / c^{+}v+$$

Where v is the functioning voltage range, c is the particular capacitance, and m is the mass. The CHI 660D electrochemical work station was utilized to direct the electrochemical exhibitions in the two arrangements, like in three terminal and two anode frameworks.

3. RESULTS AND DISCUSSION

3.1 XRD studies

The materials' "crystallite and stage underlying characterisation by means of X-beam diffraction (XRD) investigation. Nano- and sub-microspheres of Mn0.75Ni0.25CO3 (x=0.0, 0.20, 0.25, and 0.30) are shown in Figure 1 as XRD samples. Spectra of nano/sub-microspheres of MnCO3, Mn0.80Ni0.20Co3, Mn0.75Ni0.25CO3, and Mn0.75Ni0.30CO3 show diffraction peaks in the (012), (104), (110), (113), (202), (018), (116), (122) and (300) planes, corresponding to reflections located at 2 upsides of 24.25, 31.36; these peaks are all associated with the None of the nano/sub-microsphere tests with MnCO3, Mn0.80Ni0.20Co3, Mn0.75Ni0.25CO3, and Mn0.70Ni0.30CO3 showed a new peak in association with other stages such as Mn(OH)2, MnNi(OH)2, Ni(OH)2, NiCO3, or metallic Mn and Ni based stages.

The maximum power decreases with increasing Ni fixation because of the cumulative charge asymmetry caused by the Ni percentage. Scherere's [29] use of the Debye-condition yields typical crystallite diameters of 70 nm for MnCO3, 65 nm for Mn0.80Ni0.20Co3, 50 nm for Mn0.75Ni0.25CO3, and 43 nm for Mn0.70Ni0.30CO3. In Mn0.80Ni0.20Co3, Mn0.75Ni0.25CO3, and Mn0.70Ni0.30CO3, the discovery shows that Ni particles impede grain formation and prevent grain limit migration due to Zener sticking pores [30]. The pure Mn0.75Ni0.25CO3 nano/sub-microspheres with their reduced crystallite size are predicted to provide advantages for donor transport at the terminal/electrolyte interface in high-power applications."

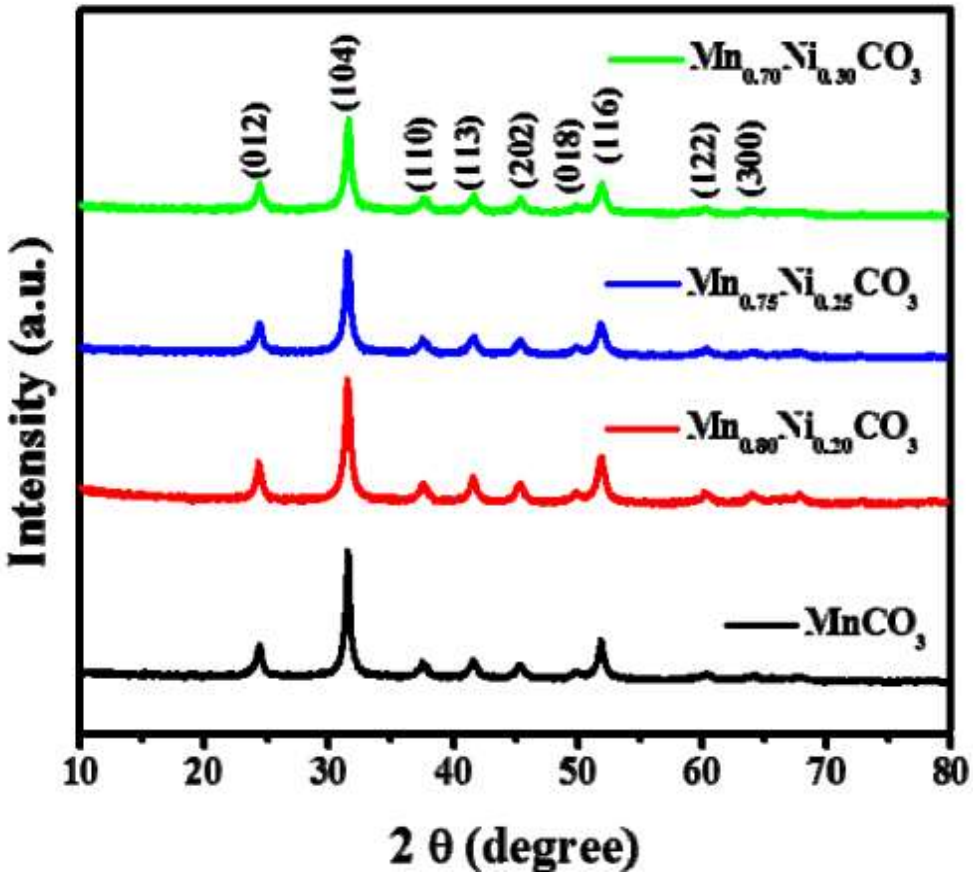

Figure-1. XRD patterns

3.2 FT-IR analysis

A following test known as Fourier change infrared spectroscopy (FT-IR) is frequently used to identify the natural and inorganic practical species present in the examples. The as-arranged MnCO3, Mn0.80Ni0.20Co3, Mn0.75Ni0.25CO3, and Mn0.70N0.30CO3 nano/sub-microspheres samples were examined using FT-IR spectroscopy

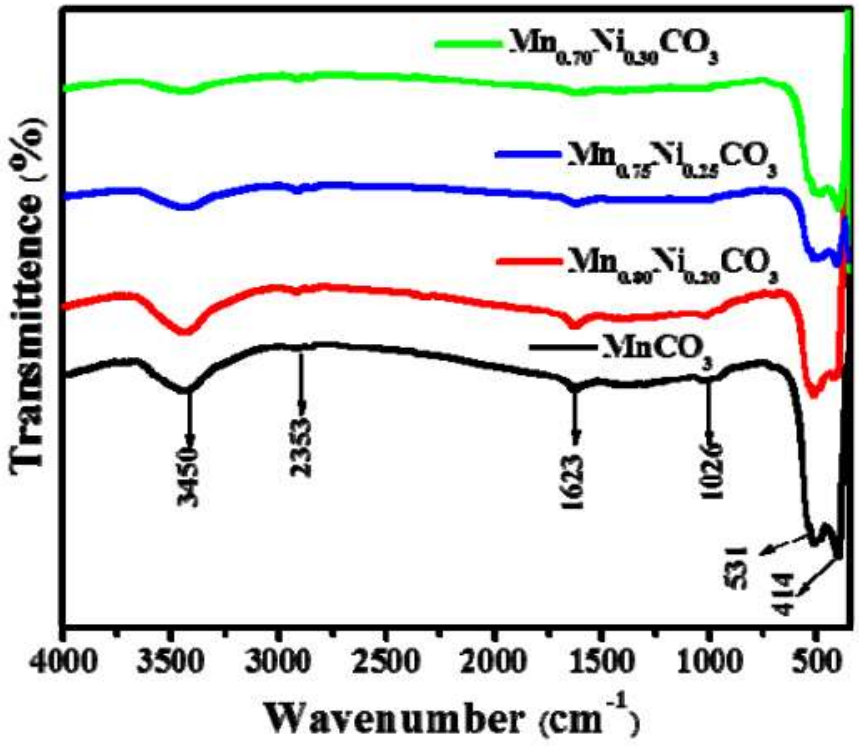

Figure-2. FT-IR spectra

The relating spectra are displayed in Figure 2. “Since Goodness and CO2 atoms can chemisorb on to the MnCO3 surface when they are presented to the air, Still present in the MnCO3 nano/sub-microspheres are water molecules. The water particles in the Mn1-xNixCO3 nano/sub-microspheres exhibit a bowing vibration that is mirrored by a band at 1623, and the Mn1-xNixCO3 tests revealed a huge top at 3450 cm-1 attributed to the O-H extending vibration. These two vibrational modes made the extra hydroxyl groupings and water on the nano/sub-microspheres visible. Less water particle adsorption is evident from the decreasing restriction of the top at 3458 cm-1 on Ni. The peak at 530 is the distinctive peak for the Mn-C-O (MnCO-Mn2+ with CO32-), while other peaks at 1026 cm-1 are attributed to the C-O extending vibration of CO32-particle and the pinnacle at 2353 cm-1 is linked to carbon dioxide [31,32]. The MnCO3 rhombohedral locations are attributed to the band between 450 and 750 cm-1. The strength of the Mn-C-O signature peak at 530 cm-1 developed during increments of 20% and 25%, the pinnacle settled, and the other peak at 414 cm-1 declined and expanded upon increases that followed. These characteristics imply that Mn0.75Ni0.25CO3 was framed homogeneously”. Both the FT-IR and XRD results show that the system and Ni affect the rhombohedral design of the MnCO3 stage.

3.3 SEM INVESTIGATION

The morphology of the framed MnCO3, Mn0.80Ni0.20Co3, Mn0.75Ni0.25CO3, and Mn0.70Ni0.30CO3 “nano/sub-microspheres were examined using SEM. The MnCO3, Mn0.80Ni0.20Co3, Mn0.75Ni0.25CO3, and Mn0.70Ni0.30CO3 nano/sub-microspheres are exceedingly homogeneously distributed and range in size from 430 to 470 nm. Given that it occurs in a carbonate media, the co-precipitation approach considers the morphological formation of nano/sub-microspheres (assimilation of carbonate arrangement with a base and the precipitation cycle all the while). The development of thermodynamically stable circle-formed MnCO3, Mn0.80Ni0.20Co3, Mn0.75Ni0.25CO3, and Mn0.70Ni0.30CO3 nano/sub-microparticles is controlled by the carbonate arrangement in these conditions. More modest crystallites form when the modest Ni2+ particle (70 pm) with the larger Mn2+ particle cross section (81 pm) receives the gems. The aftereffects of XRD, FT-IR, and SEM are predictable with each other. With an expansion in Ni2+ focus, surface unpleasantness likewise rises, as would be considered normal to bring about a more noteworthy capacitance and a faster trade of electrons on a superficial level.”

3.4 TEM Evaluation

TEM images "of nano/sub-microspheres of MnCO3 and Mn0.75Ni0.25CO3 at various amplifications. Regarding the form and nature of the accumulation of the nanospheres, these images are in excellent agreement with the SEM micrographs. The nano/sub-microspheres are 430 nm (MnCO3) and 450 nm in breadth (Mn0.75Ni0.25CO3). In Figures C and F, it was shown that the grid distances for MnCO3 and Mn0.75Ni0.25CO3 nano/sub-microspheres were, respectively, 7.4 and 7.2. The inset images of the MnCO3 and Mn0.75Ni0.25CO3 exhibited apparent patches arranged, and the cross section finger values are then well in accord with (104) planes. For applications utilising supercapacitors, improved electrochemical performance is enabled by the presence of pores on both nanosphere surfaces that can provide efficient electron and particle transport."

3.5 Electrochemical performance of solid-state $Mn_{0.75}Ni_{0.25}CO_3$//GNS asymmetric supercapacitor

We developed a strong state ASC device using graphene nanosheets as the negative terminal, PVA-Na2SO4 as the strong state electrolyte, and Mn0.75Ni0.25CO3 nano/sub-microspheres as the positive cathode to further assess the practical usefulness of the material. "The strong state ASC was created using GNS as the negative cathode, and its specific capacitance is 115 F g-1 at 1 A g-1, according to charge/release bending. The steady voltage windows for the GNS and Mn0.75Ni0.25CO3 nano/sub-microsphere, respectively, are currently unknown and are expected to be -1.0 V to 0.0 V and 0.0 V to 1.0 V. The cathode CV bends of these materials. The strong state ASC device exhibits a capacitive behaviour at a few functioning probable windows between 0.0 V and 2.2 V at 50 mV s-1, with nearly rectangular CV bends and no discernible redox top. The results of evaluating the impact of output rates for a strong state ASC device in the voltage range of 0 to 2.0 V at various output rates ranging from 10 to 100 mV s-1. In fact, even at a faster checking speed of 100 mV s-1, the cell's ASC device CV profile has maintained a broadly rectangular shape with essentially no other disruptions in the two-layer conduct. It is anticipated that this electrochemical characteristic, which was made possible by the anode/electrolyte interfacial uniqueness during manufacturing, will provide excellent charge/release qualities with increased rate capacity. The capability of the charge-release profile plainly concentrates to a longer release duration when the galvanostatic charge-release (GCD) bends at different current densities. Release bends at separate current densities of 0.5, 1.0, 2.0, 3.0, 5.0, 7.0, and 9.0 A g-1 are used to determine the specific capacitance. Additionally, after 7500 cycles of charge-release at the higher current thickness of 3 A g-1, 88% capacitance maintenance was still maintained, demonstrating its high rate limit. It's possible that the stable nano/sub-microspheres morphology and construction of the terminal materials created during the union of the antecedent by sodium bicarbonate, where the nanoparticles surface roughness gives more dynamic surface region, less obstruction for electron/particle transport at the cathode/electrolyte connection point, and stable stage structure, is the cause of this limit ability"

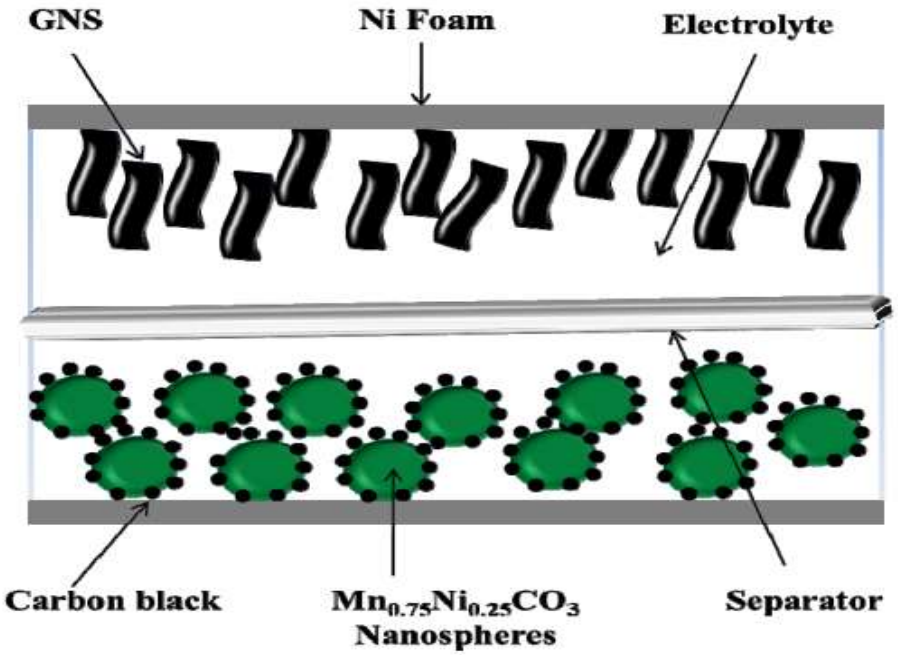

maintenance..

FIGURE -3. SOLID-STATE ASYMMETRIC SUPERCAPACITOR CONFIGURATION

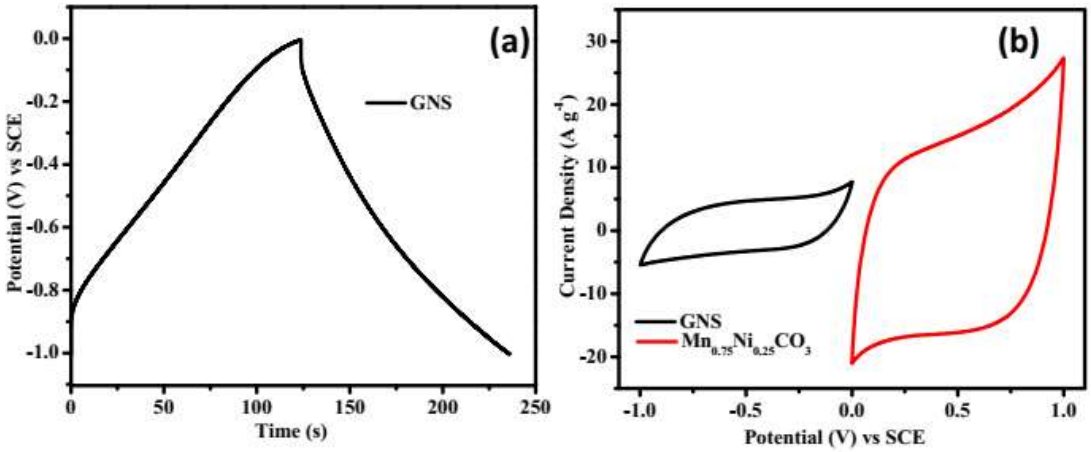

Figure-4 charge discharge curve of GNS at a current density

Because of the steady anode and electrolyte designs, there was little variety in the charge move obstruction and electrolyte opposition values for the ASC gadget when the electrochemical impedance spectra were estimated when 7500 cycles. Here, we give the energy thickness and Mn0.75Ni0.25CO3/GNS ASC power thickness in the Ragone plot. These two boundaries, which are measurable, are indicative of an ASC operating at a high level of execution.

"Where E, Cs, V, P, and t are the release potential (V), power thickness (kW kg-1), release time (s), explicit capacitance (F g-1), energy thickness (Wh kg-1), and the sum of the above-mentioned components, respectively. The red-light producing diode (Drove) might be lit using the Mn0.75Ni0.25CO3/GNS ASC device after it has been charged (see Figure 8.19 b). When the power thickness increases from 499 to 15840 W kg-1, the energy thickness of the manufactured ASC decreases from 25 to 12.22 W h kg-1. Nanostructured Mn0.75Ni0.25CO3 strong state ASC shown exceptional electrochemical performance because to their unique size impact, large surface area, low thickness, and Na+ particle entrance in the Mn0.75Ni0.25CO3 nano/sub-microspheres cathodes."

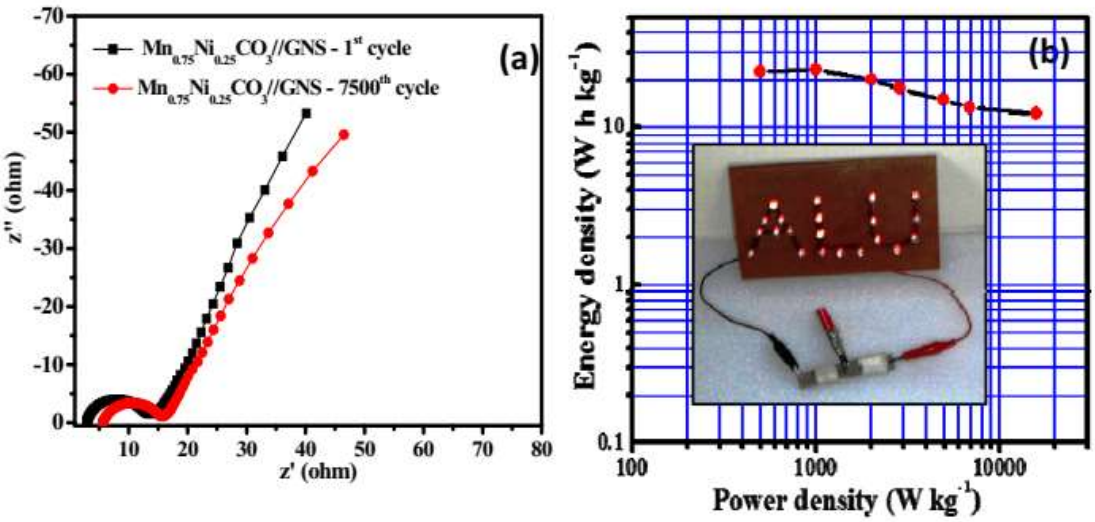

Figure-5. (a) EIS curves (b) Ragone plots

The exhibition of Mn-based ASC terminal materials is looked at in the couple of papers that are at present accessible. Most essentially, this worth is adequate to meet the power necessities for the PNGV. At lower current densities of 0.5 A g-1 and 9 A g-1, separately, 499 W kg-1 and 15540 W kg-1 power densities, individually, were found (Organization for Another Age of Vehicles). "These discoveries showed that the strong state Mn0.75Ni0.25CO3/GNS ASC gadget has a ton of potential for true use. The uniform nano/sub-microsphere morphology as the cathode and more surface area of GNS as the anode material, which make them more available to more modest electrolytic particles and positive for the quick dispersion of the electrolyte particles at the outer layer of terminal materials, are the reasons for the high energy and power thickness of strong state ASC applications anode materials. During the intermittent consolidation/extraction process, the strong state ASC terminal materials guard against limit

corruption. The Mn0.75Ni0.25CO3/GNS strong state ASC gadget that is being featured is imaginative, reasonable, easy to make, and has great potential for energy and power thickness gadgets."

3.6 "POWER DENSITY, POTENTIAL WINDOW, AND SPECIFIC CAPACITY OF THE REPORTED WORK ON MN BASED ASYMMETRIC SUPERCAPACITORS."

Material Name	Specific capacitance ($F\ g^{-1}$)	Potential window	Current density	Energy density ($Wh\ kg^{-1}$)	Powerdensity ($W\ kg^{-1}$)
$MnCO_3$@MnO_2	60.8	1.8 V	0.3 A g^{-1}	27.4 3	271.7
MnO_2//AG	50	1.0 V	0.25 A g^{-1}	22.5	146.2
MnO_2/La_2O_3//AC	46	2.0 V	0.3 A g^{-1}	25.8	0.3
PM//HMC	48	1.6 V	1.08 mA g^{-1}	14.7	90
CNFs//MnO_2	45	1.8 V	0.5 A g^{-1}	20.3	485
Mn0.75Ni0.25CO3 //GNS	**46**	**2.0 V**	**0.5 A g^{-1}**	**25**	**499 W kg^{-1}**

4. CONCLUSIONS

We have summarised a fundamental co-precipitation method that considers the quick layout initial free mix of Mn1-xNixCO3 (x-0, 0.20,0.25 and 0.30) nano/sub-microspheres. "According to tests using infinitesimal and X-beam diffraction techniques, the supplied rhombohedral Mn1-xNixCO3 particles had homogeneously scattered glasslike nano/sub-microsphere morphologies with sizes between 430 and 470 nm. The limit supplied by MnCO3 in 1 M of Na2SO4 electrolyte was outperformed by 23.07% to a high unambiguous limit of 364 F g-1 by the Mn0.75Ni0.25CO3 nano/sub-microsphere terminal. The Mn0.75Ni0.25CO3 nano/sub-microspheres cathode is one of the promising terminals for long haul cycle soundness due to its supported presentation at 5 A g-1 more than 7500 cycles. A power thickness of 499 W kg-1 was also demonstrated by the Mn0.75Ni0.25CO3/GNS deviated supercapacitor device at a high unambiguous energy thickness of 25 Wh kg-1. Additionally, the strong state ASC maintained 88% capacitance even after 7500 cycles, which is a bonus and appropriate for commercial applications. Additionally, the development of new Li-particle anode, sensor, and photocatalyst applications has a new path thanks to the Mn0.75Ni0.25CO3 nano/sub-microsphere materials. The continuous utilization of petroleum products, which are a limited wellspring of energy and the essential wellspring of energy around the world, hurts the biological system. It is important to track down substitute wellsprings of energy, and a great deal of examination is right now being finished on feasible energy innovations like sun

oriented, biomass, wind, hydropower, geothermal power, sea energy, and hydrogen fuel delivered from the sun. Capacity frameworks were essential to create energy from the previously mentioned sources reasonably, earth, and financially. In such manner, the issue of how issues and requests for energy capacity advancements will be met in what's to come emerges. The Li-particle battery and supercapacitor advancements are the best energy stockpiling choices for purchaser applications. In view of their high energy, high voltage, exceptional cycle life, and phenomenal stockpiling characteristics, Li-particle batteries and Supercapacitors have displaced other energy stockpiling advances as the most well known choices for electronic vehicle applications."

REFERENCES

1. L. Liu, Z. Yang, H. Liang, H. Yang and Y. Yang, Mater. Lett. **64**, 2060(2010).
2. S. Nagamuthu, S. Vijayakumar and G. Muralidharan, Energy & Fuels **27**,3508 (2013).
3. G. Settanni, J. Zhou, T. Suo, S. Schöttler, K. Landfester, F. Schmid and V.Mailänder, Nanoscale **7**, 10146 (2015).
4. L. Zhou, X. Kong, M. Gao, F. Lian, B. Li, Z. Zhou and H. Cao, Inorg. Chem. **53**, 9228 (2014).
5. Q. X. Xia, K. San Hui, K. N. Hui, S. D. Kim, J. H. Lim, S. Y. Choi, L. J. Zhang, R. S. Mane, J. M. Yun and K. H. Kim, J. Mater. Chem. A **3**, 22102 (2015).
6. C. Ding, D. Yan, Y. Zhao, Y. Zhao, H. Zhou, J. Li and H. Jin, Phys. Chem. Chem. Phys. **18**, 25879 (2016).
7. L. Xiao, S. Wang, Y. Wang, W. Meng, B. Deng, D. Qu, Z. Xie and J. Liu,ACS Appl. Mater. Interfaces **8**, 25369 (2016).
8. J. K. Heuer and J. F. Stubbins, Corros. Sci. **41**, 1231 (1999).
9. B. Wei, L. Wang, Q. Miao, Y. Yuan, P. Dong, R. Vajtai and W. Fei, CarbonN. Y. **85**, 249 (2015).
10. R. Madhuvilakku, S. Alagar, R. Mariappan and S. Piraman, Sensors Actuators,B Chem. **253**, 879 (2017).
11. Z. Lei, F. Shi and L. Lu, Appl. Mater. Interfaces **4**, 1058−1064 (2012).
12. J. W. Lee, A. S. Hall, J. D. Kim and T. E. Mallouk, Chem. Mater. **24**, 1158(2012).
13. S. Nagamuthu, S. Vijayakumar and G. Muralidharan, Energy & Fuels **27**,3508 (2013).
14. K. Subramani, D. Jeyakumar and M. Sathish, Phys. Chem. Chem. Phys. **16**,4952 (2014).
15. S. H. Lee, Y. Kwon, S. Park, M. Cho and Y. Lee, J. Mater. Sci. **50**, 5952(2015).
16. Z. Bai, H. Li, M. Li, C. Li, X. Wang, C. Qu and B. Yang, Int. J. HydrogenEnergy **40**, 16306 (2015).
17. J. Yuan, J. Zhu, H. Bi, Z. Zhang, S. Chen, S. Liang and X. Wang, RSC Adv. **3**,4400 (2013).
18. Y. Li, B. Guan, A. Maclennan, Y. Hu, D. Li, J. Zhao, Y. Wang and H. Zhang,Electrochim. Acta **241**, 395 (2017).
19. Y. Tang, S. Chen, T. Chen, W. Guo, Y. Li, S. Mu, S. Yu, Y. Zhao, F. Wen andF. Gao, J. Mater. Chem. A **5**, 3923 (2017).
20. Y. Zhang, Y. Zhang, Y. Zhang, H. Si and L. Sun, Nano-Micro Lett. **11**, 35(2019).
21. P. Ning, X. Duan, X. Ju, X. Lin, X. Tong, X. Pan, T. Wang and Q. Li,Electrochim. Acta **210**, 754 (2016).
22. H. Chen, Z. Yan, X. Y. Liu, X. L. Guo, Y. X. Zhang and Z. H. Liu, J. PowerSources **353**,

202 (2017).
23. R. Rajendiran, D. Chinnadurai, A. R. Selvaraj, R. K. Gunasekaran, H. J. Kim, S. Karupannan and K. Prabakar, Electrochim. Acta **297**, 77 (2019).
24. S. Devaraj, H. Y. Liu and P. Balaya, J. Mater. Chem. A **2**, 4276 (2014).
25. Y. Zhang, Y. Zhang, Y. Zhang, H. Si and L. Sun, Nano-Micro Lett. **11**, 35(2019).
26. H. K. Lee, D. Sakemi, R. Selyanchyn, C. G. Lee and S. W. Lee, ACS Appl. Mater. Interfaces **6**, 57 (2014).
27. S. Alagar, R. Madhuvilakku and R. Mariappan, J Mater Sci Mater Electron **29**,1173 (2018).
28. F. J. Humphreys and M. G. Ardakani, Acta Mater. **44**, 2717 (1996).